Figure S1, related to Figure 1.

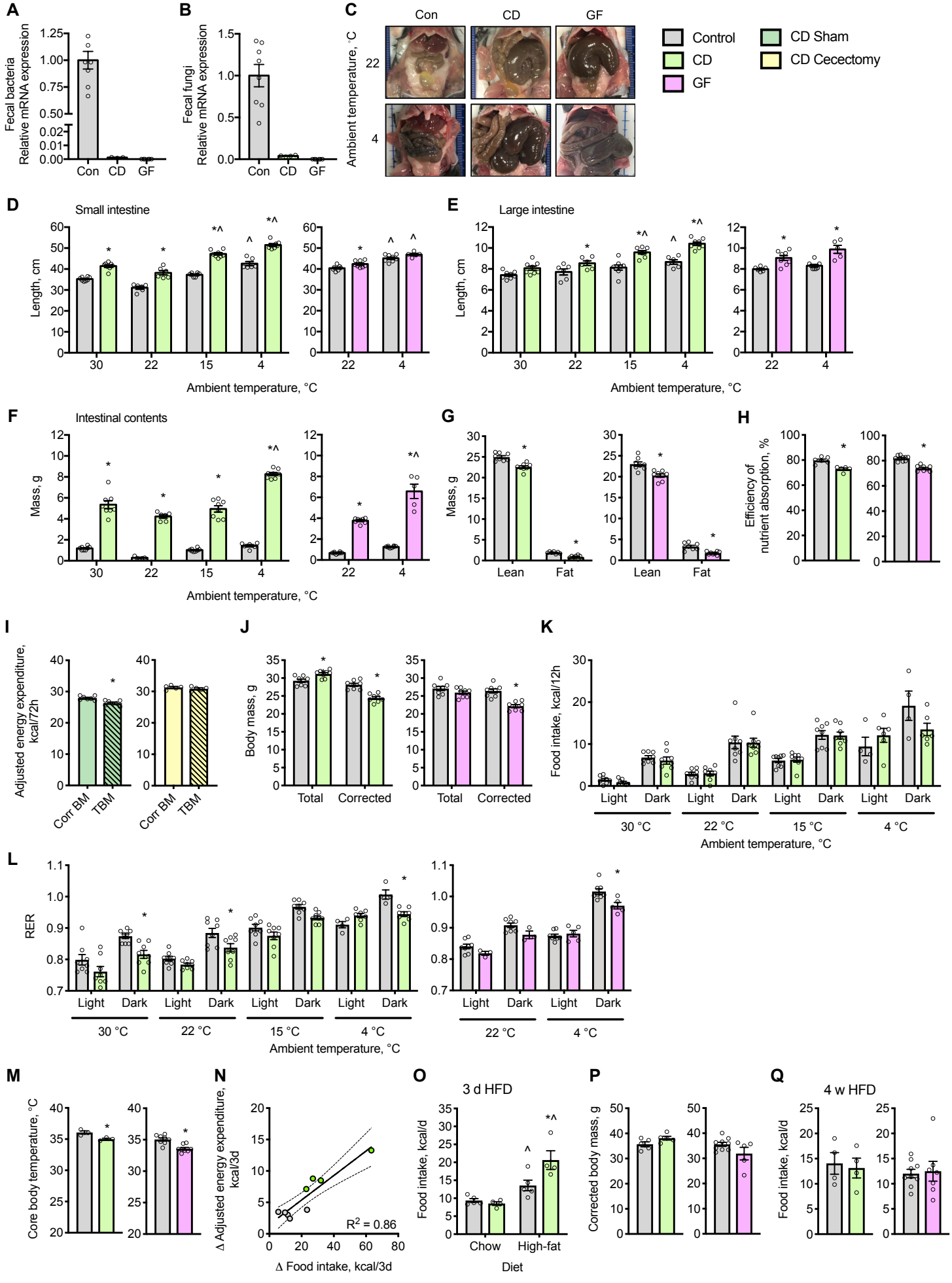

Figure S1, related to Figure 1: The gut microbiome is dispensable for both cold- and diet-induced thermogenesis.

(A and B) The deficiency of the gut microbiome in commensal depleted (CD) and germ-free (GF) mice was confirmed by qPCR for fecal bacteria (A) and fungi (B) (*n* = 4-8).

(C) Representative images of the peritoneal cavity in chow fed mice housed at 22 °C (*n* = 8).

(D-F) Lengths of (D) small and (E) large intestines and (F) masses of intestinal contents in mice housed at 22 °C or acclimated to different ambient temperatures (*n* = 5-8).

(G) Lean and fat masses of mice housed at 22 °C (*n* = 7-8).

(H) Efficiency of nutrient absorption over 24 h in mice housed at 22 °C (*n* = 5-10).

(I) Values of energy expenditure adjusted by ANCOVA for corrected body mass (Corr BM) or total body mass (TBM) in mice housed at 22 °C following cecectomy or sham surgery (*n* = 5-7).

(J) Total and corrected body mass in mice housed at 22 °C (*n* = 7-8).

(K and L) Total food intake (K) and average RER values (L) during the light and dark phases (*n* = 5-8).

(M) Core body temperatures in mice housed at 22 °C (*n* = 3-8).

(N) Correlation between the changes (∆) in food intake and energy expenditure in response to 3 d palm oil-based HFD feeding. Solid and dashed lines represent linear regression and 95% confidence intervals respectively (*n* = 4-5).

(O) Average daily food intake during 3 d prior to and following HFD feeding (related to Figure 1F) (*n* = 4-5).

(P and Q) Corrected body mass (P) and average daily food intake (Q) measured over 3 d in mice following palm oil-based HFD feeding for 4 w while housed at 30 °C (related to Figure 1G) (*n* = 4-8).

Circles represent individual mice; Barplots represent means ± s.e.m. Statistical analyses were conducted using Student's *t*-test or 2-way ANOVA with repeated measures where appropriate. **P* < 0.05 control *vs.* CD or GF mice, ^*P* < 0.05 within group comparisons.

Figure S2, related to Figure 2.

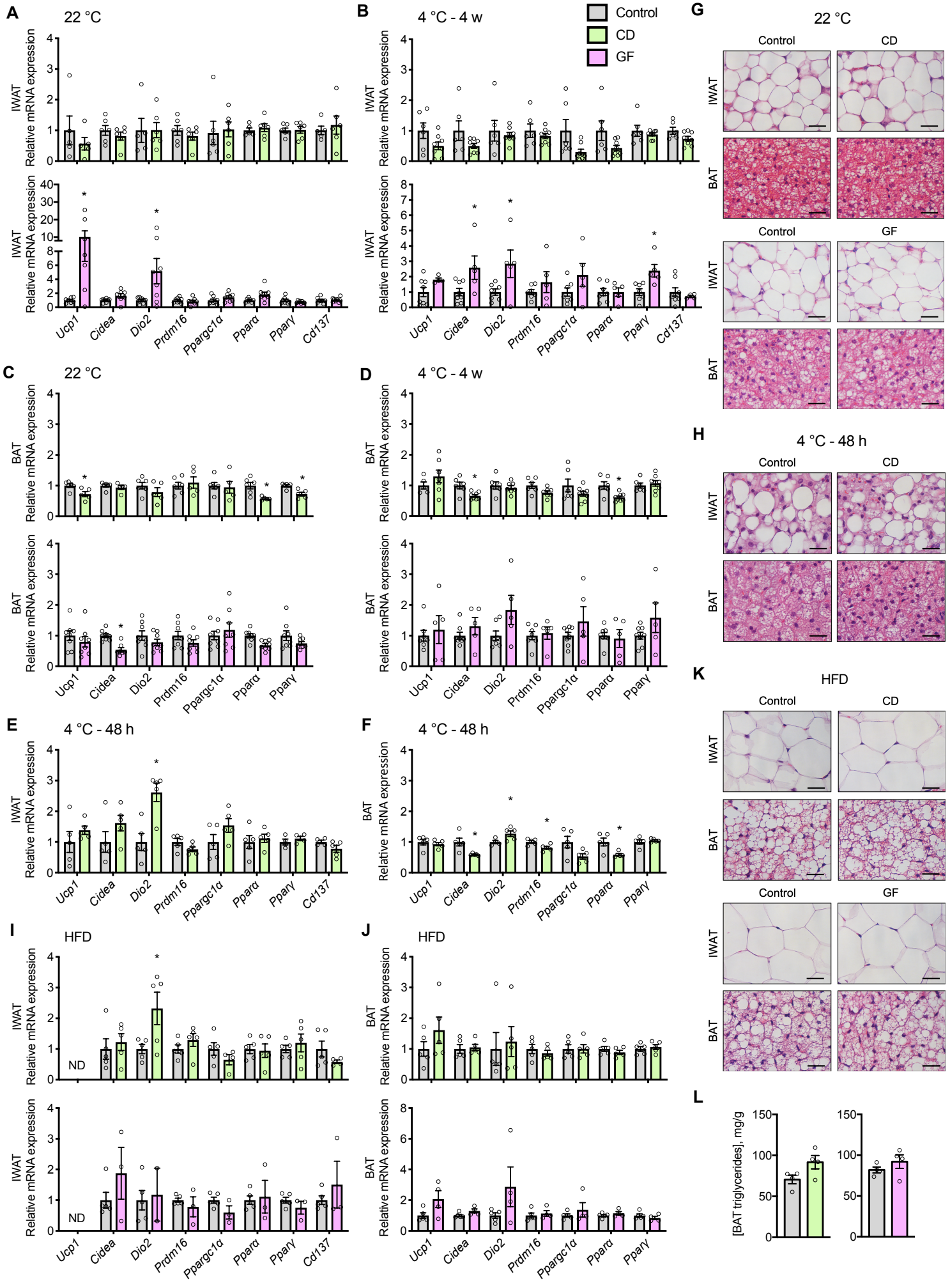

Figure S2, related to figure 2: The gut microbiome is not required for recruitment and activation of thermogenic tissues.

(A and B) Steady state mRNA levels of transcription factors and other thermogenic gene markers in IWAT of CD (40 d antibiotics) and GF mice, (A) housed at 22 °C or (B) acclimated to 4°C (4 w) (*n* = 5-8).

(C and D) Steady state mRNA levels of transcription factors and other thermogenic gene markers in BAT of CD (40 d antibiotics), and GF mice, (C) housed at 22 °C or (D) acclimated to 4°C (4 w) (*n* = 5-8).

(E and F) Steady state mRNA levels of transcription factors and other thermogenic gene markers in (E) IWAT and (F) BAT of CD mice exposed to 4°C for 48 h (*n* = 4-5).

(G and H) Representative H&E staining of IWAT and BAT from mice fed a chow diet and acclimated to (G) 22 °C or (H) housed at 4 °C for 48h; Scale bar = 50 μM (*n* = 4-5).

(I and J) Steady state mRNA levels of transcription factors and other thermogenic gene markers in (I) IWAT and (J) BAT of mice acclimated to 30 °C and fed a palm oil-based HFD for 4 w (*n* = 3-5).

(K) Representative H&E staining of IWAT and BAT from mice acclimated to 30 °C and fed a palm oil-based HFD for 4 w; Scale bar = 50 μM (*n* = 3-5).

(L) Triglyceride concentrations in BAT (*n* = 4).

Circles represent individual mice; Barplots represent means ± s.e.m. Statistical analyses were conducted using Student's *t*-test; **P* < 0.05 control *vs.* CD or GF mice.

Figure S3, related to Figure 3.

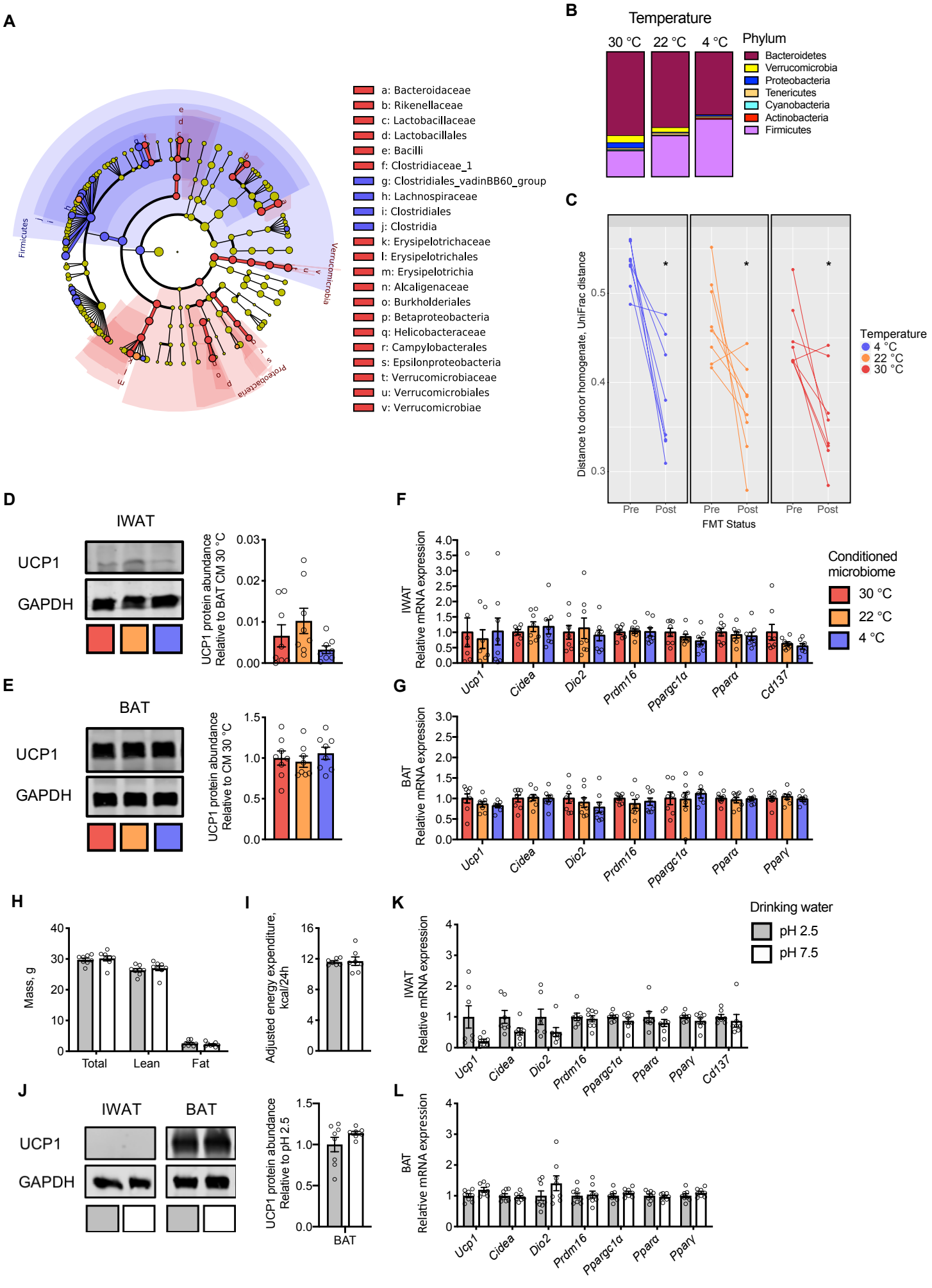

Figure S3, related to Figure 3: Temperature-conditioned gut microbiota do not influence cold- or diet-induced thermogenesis.

(A) Fecal microbiota cladogram showing taxa associated via LEfSe with each temperature group of donors (red, 30 °C; blue, 4 °C) (*n* = 4-8).

(B) Predominant phyla of fecal gut microbiota from donor mice fed chow and acclimated to different ambient temperatures (*n* = 4-8).

(C) The change in UniFrac distance between microbiota of recipient mice and their respective temperature-conditioned donor homogenate as a function of FMT status (*n* = 8).

(D-G) Recipient mice were housed at 22 °C and fed chow for 4 w following FMT. Representative immunoblots and quantification of UCP-1 protein in (D) IWAT and (E) BAT, and steady state mRNA levels of transcription factors and other thermogenic gene markers in (F) IWAT and (G) BAT (*n* = 7-8).

(H-L) Chow fed mice housed at 22 °C and receiving acidified (pH 2.5) or neutral (7.5) water. (H) Total, lean and fat mass and (I) energy expenditure. (J) Representative immunoblots of UCP1 protein expression in IWAT and BAT and quantification of Ucp-1 in BAT (not detected in IWAT). Steady state mRNA levels of transcription factors and other thermogenic gene markers in (K) IWAT and (L) BAT (*n* = 7-8).

Circles represent individual mice; Barplots represent means ± s.e.m; Statistical analyses were conducted using paired (C) or unpaired (H-L) Student's *t*-test or (D-G) 1-way ANOVA; **P* < 0.05 pre- *vs.* post-FMT.

Figure S4, related to Figure 4.

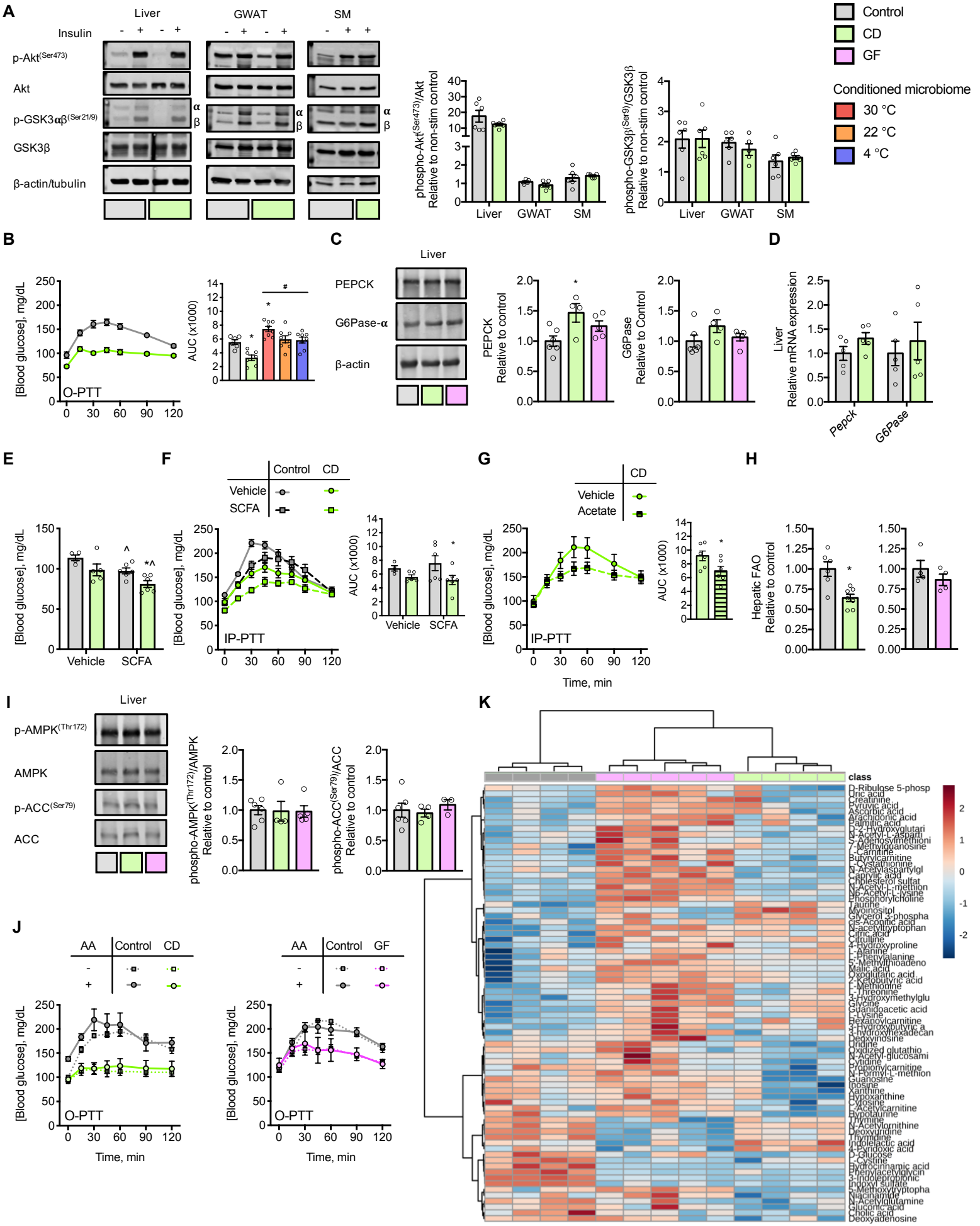

Figure S4, related to Figure 4: The gut microbiome promotes hepatic gluconeogenesis.
(A) Mice fasted for 6 h were administered insulin (1 U/kg) via inferior vena cava and sacrificed after 4 min for the quantification of insulin signaling proteins in the liver, GWAT and skeletal muscle (SM). Representative immunoblots are displayed. β-actin (liver and GWAT) and β-tubulin (SM) were used as controls for unequal loading (*n* = 6).
(B) Mice housed at 22 °C were subjected to O-PTT. Inset barplots represent AUC values. Not displayed are curves for mice with temperature-conditioned gut microbiota (*n* = 6-8).
(C and D) Hepatic protein levels (C) and mRNA expression (D) of the gluconeogenic enzymes PEPCK and G6Pase in mice fasted for 6 h. Representative immunoblots are displayed with β-actin used as a control for unequal loading (*n* = 5-6).
(E-G) Mice were supplemented with SCFAs or acetate alone in their drinking water for 1 w, fasted for 6 h, and then subjected to measurements of (E) blood glucose concentrations and (F and G) IP-PTT. Inset barplots represent AUC values (*n* = 5-6).
(H) Rates of hepatic FAO (*n* = 4-7).
(I) Representative immunoblots and quantification of phosphorylated and total AMPK and ACC, which regulate FAO (*n* = 3-6).
(J) O-PTT in mice prior to and following amino acid (AA) supplementation (*n* = 4-7).
(K) Unsupervised Ward/Pearson cluster heat map of portal vein serum (PVS) samples based on top 75 metabolites ranked by ANOVA. Heatmap color scale represents the highest (red) and lowest (blue) metabolite peak intensities following log transformation and auto-scaling (*n* = 4-5).
All mice were fed a chow diet and housed at 22 °C. Circles represent individual mice; Barplots and points joined by lines represent means ± s.e.m. Statistical analyses were conducted via Students *t*-test, 1- or 2-way ANOVA where appropriate; *$P < 0.05$ control *vs.* CD or GF mice, ^$P < 0.05$ within group comparisons.

°C	Measurement	Control	CD	*P*-value	Control	GF	*P*-value
Chow diet: Related to Figure 1 and S1							
30	Total body mass, g	26.7 ± 0.4	27.3 ± 0.5	0.298			
	Corrected body mass, g	25.5 ± 0.3	22.0 ± 0.6	***0.000***			
	Corrected body mass, % TBM	95.6 ± 0.2	80.4 ± 1.4	***0.000***			
	Lean mass, g	22.3 ± 0.3	19.7 ± 0.5	***0.001***			
	Fat mass, g	2.51 ± 0.16	1.55 ± 0.09	***0.000***			
	Core body temperature, °C	35.4 ± 0.2	34.4 ± 0.1	***0.001***			
15	Total body mass, g	26.7 ± 0.6	26.8 ± 0.4	0.794			
	Corrected body mass, g	25.4 ± 0.6	21.9 ± 0.3	***0.000***			
	Corrected body mass, % TBM	95.4 ± 0.8	81.6 ± 1.0	***0.000***			
	Lean mass, g	22.9 ± 0.6	19.5 ± 0.2	***0.000***			
	Fat mass, g	1.86 ± 0.06	1.49 ± 0.07	***0.002***			
	Core body temperature, °C	35.7 ± 0.2	34.4 ± 0.2	***0.002***			
4	Total body mass, g	28.7 ± 1.0	31.1 ± 0.4	***0.035***	25.8 ± 0.3	28.6 ± 1.2	0.892
	Corrected body mass, g	27.3 ± 0.9	22.9 ± 0.4	***0.000***	24.6 ± 0.3	22.1 ± 0.6	***0.002***
	Corrected body mass, % TBM	95.1 ± 0.3	73.4 ± 0.5	***0.000***	95.1 ± 0.1	77.3 ± 1.6	***0.000***
	Lean mass, g	24.8 ± 0.89	20.6 ± 0.32	***0.000***	21.9 ± 0.3	19.6 ± 0.5	***0.002***
	Fat mass, g	2.32 ± 0.15	1.69 ± 0.04	***0.001***	2.09 ± 0.1	1.74 ± 0.1	***0.006***
	Core body temperature, °C	36.1 ± 0.4	35.4 ± 0.3	0.173	35.1 ± 0.3	34.6 ± 0.4	0.329
	Physical activity, m/24h	239 ± 23	114 ± 9	***0.000***	196 ± 18	153 ± 20	0.141

°C	Measurement	30 °C CM	22 °C CM	4 °C CM	*P*-value
Chow diet-fed recipient mice: Related to Figure 3 and S3					
22	Total body mass, g	26.6 ± 0.4	26.8 ± 0.4	27.2 ± 0.4	0.581
	Lean mass, g	22.2 ± 0.3	22.5 ± 0.3	22.8 ± 0.4	0.472
	Fat mass, g	2.75 ± 0.17	2.72 ± 0.10	2.87 ± 0.12	0.712
	Core body temperature, °C	36.4 ± 0.1	36.0 ± 0.1	36.2 ± 0.1	0.200
	Small intestine length, cm	42.6 ± 1.2	42.0 ± 0.8	43.7 ± 0.7	0.415
HFD-fed recipient mice: Related to Figure 3					
30	Total body mass, g	39.1 ± 1.8	38.5 ± 1.3	38.4 ± 1.4	0.939
	GWAT, g	1.95 ± 0.14	1.88 ± 0.11	2.05 ± 0.12	0.662
	Core body temperature, °C	35.4 ± 0.2	35.2 ± 0.2	35.5 ± 0.2	0.753
	Small intestine length, cm	37.0 ± 0.7	36.9 ± 0.3	36.2 ± 0.5	0.514

Table S1, related to Figure 1 and S1 and Figure 3 and S3: Mouse characteristics.

(Top) Control, CD and GF mice were fed a chow diet and acclimated (4 w) to ambient temperatures. Corrected body mass (body mass without intestinal contents) is provided in grams and as a percentage of TBM (total body mass).

(Bottom) Mice received a FMT with conditioned microbiome (CM) from mice acclimated (4 w) to 30, 22 or 4 °C, and were then fed either chow or lard-based HFD and housed at 22 °C or 30 °C, respectively. Blank cells indicate that experiments were not conducted. Values represent means ± s.e.m (*n* = 6-8).

Statistical analyses were conducted using Student's *t*-test (top) or 1-way ANOVA (bottom); $P < 0.05$ control *vs.* CD or GF mice (bold and italicized).

	Report	Relative abundance, %			Change, %		
		Ambient temperatures, °C			29-30 *vs.*	29-30 *vs.*	17-22 *vs.*
		29-30	17-22	4-12	17-22 °C	4-12 °C	4-12 °C
Abundant phyla							
Bacteroidetes	Krisko *et al.*	67.0 ± 3.9	60.7 ± 8.0	50.5 ± 4.5	-9.5	-24.7	***-16.8***
	Chevalier *et al.*		72.7 ± 4.6	35.3 ± 4.2			***-51.5***
	Zietak *et al.*	13.9 ± 1.5	21.7 ± 2.9	19.6 ± 3.0	56.3	40.8	***-10.0***
Firmicutes	Krisko *et al.*	20.7 ± 1.4	32.7 ± 7.2	45.9 ± 4.4	57.8	121.3	***40.3***
	Chevalier *et al.*		18.6 ± 5.3	60.5 ± 4.1			***224.9***
	Zietak *et al.*	80.9 ± 1.4	73.5 ± 3.4	76.8 ± 3.3	-9.1	-5.1	***4.5***
Tenericutes	Krisko *et al.*	1.3 ± 0.3	1.6 ± 0.6	1.3 ± 0.6	30.3	2.6	***-21.3***
	Chevalier *et al.*		0.7 ± 0.3	0.6 ± 0.3			***-21.7***
	Zietak *et al.*	0.02 ± 0.01	0.04 ± 0.02	0.12 ± 0.06	97.2	415.0	161.2
Proteobacteria	Krisko *et al.*	4.2 ± 1.0	0.8 ± 0.2	1.2 ± 0.2	-80.9	-72.0	45.6
	Chevalier *et al.*		1.5 ± 0.1	1.0 ± 0.1			***-31.9***
	Zietak *et al.*	3.6 ± 0.6	4.1 ± 0.7	2.9 ± 0.3	13.9	-18.4	***-28.4***
Actinobacteria	Krisko *et al.*	0.2 ± 0.1	0.5 ± 0.2	1.1 ± 0.7	111.7	381.9	127.7
	Chevalier *et al.*		0.02 ± 0.00	0.01 ± 0.00			***-40.3***
	Zietak *et al.*	1.3 ± 0.6	0.6 ± 0.1	0.2 ± 0.1	-50.1	-80.6	***-61.2***
Verrucomicrobia	Krisko *et al.*	5.76 ± 3.0	3.68 ± 3.5	0.03 ± 0.03	-36.0	-99.4	***-99.1***
	Chevalier *et al.*		5.96 ± 2.4	0.00 ± 0.00			***-100.0***
	Zietak *et al.*	0.39 ± 0.25	0.00 ± 0.00	0.27 ± 0.23	-99.8	-29.9	28745.6
Cyanobacteria	Krisko *et al.*	0.80 ± 0.41	0.02 ± 0.02	0.02 ± 0.02	-97.3	-97.6	-12.5
	Chevalier *et al.*		0.36 ± 0.09	0.54 ± 0.07			50.7
	Zietak *et al.*	ND	ND	ND			
Metabolically notable populations							
Erysipelotrichaceae	Krisko *et al.*	4.8 ± 1.2	3.4 ± 0.9	0.5 ± 0.1	-30.1	-89.0	***-84.2***
	Chevalier *et al.*		0.7 ± 0.3	0.0 ± 0.0			***-95.9***
	Zietak *et al.*	25.3 ± 1.0	0.6 ± 0.3	0.4 ± 0.1	-97.4	-98.4	***-47.5***
Lachnospiraceae	Krisko *et al.*	4.2 ± 1.0	15.8 ± 5.8	27.0 ± 4.0	273.2	538.3	***71.0***
	Chevalier *et al.*		1.3 ± 0.3	4.7 ± 0.5			***256.1***
	Zietak *et al.*	39.7 ± 1.0	58.8 ± 0.3	63.6 ± 5.2	48.2	60.3	***8.2***
Akkermansia muciniphila	Krisko *et al.*	5.8 ± 3.0	3.7 ± 3.5	0.0 ± 0.0	-36.0	-99.4	***-99.1***
	Chevalier *et al.*		6.0 ± 2.3	0.0 ± 0.0			***-100.0***
	Zietak *et al.*	0.4 ± 0.2	0.0 ± 0.0	0.3 ± 0.2	-99.8	-29.9	28745.6
Lactobacillus	Krisko *et al.*	1.4 ± 0.3	0.5 ± 0.3	0.0 ± 0.0	-63.3	-100.0	***-100.0***
	Chevalier *et al.*		0.0 ± 0.0	0.0 ± 0.0			***-58.1***
	Zietak *et al.*	7.6 ± 2.6	2.6 ± 0.9	4.3 ± 1.8	-65.3	-42.5	65.6

Table S2, related to Figure 3 and S3: Microbial composition in response to altered ambient temperature.

Microbiome comparisons were made between the present study (Krisko et al., 2020) and publicly available data (Chevalier et al., 2015, Zietak et al., 2016). Mice were grouped according to exposure to thermoneutral temperatures 29-30 °C (Krisko et al., 30 °C; Zietak et al., 29 °C), and increasing cold ambient temperatures of 17-22 °C (Krisko et al., 22 °C; Chevalier et al., room temperature; Zietak et al., 17 °C) and 4-12 °C (Krisko et al., 4 °C; Chevalier et al., 6 °C; Zietak et al., 12 °C). ND, not detected. Blank cells indicate data that were not collected. Values represent means of relative abundance ± s.e.m (*n* = 4-8). Bold and italicized values indicate common trends among two or more studies.

KEGG code	Dysregulated metabolites in liver	Direction of dysregulation	Fold change	
			CD	GF
Saline				
C00212	Adenosine	Increased	1.55	1.30
C00262	Hypoxanthine	Decreased	0.74	0.81
C04282	1-Pyrroline-4-hydroxy-2-carboxylate*	Decreased	0.72	0.58
C00025	Glutamate	Decreased	0.70	0.58
C00065	Serine	Decreased	0.56	0.67
C00049	Aspartate	Decreased	0.60	0.57
Pyruvate				
C00352	Glucosamine phosphate	Increased	8.57	5.23
C02488	Ethyl malate*	Increased	4.14	2.28
C00900	Acetolactate*	Increased	3.21	1.87
C01172	Hexose phosphates*	Increased	1.76	1.93
C02225	Methylcitrate*	Increased	1.65	1.97
C00212	Adenosine	Increased	1.82	1.55
C00026	Ketoglutarate	Increased	1.79	1.37
C00122	Fumarate	Decreased	0.68	0.76
C00546	Methylglyoxal*	Decreased	0.59	0.78
C00149	Malate	Decreased	0.63	0.74
C00065	Serine	Decreased	0.58	0.76
C01697	Galactitol*	Decreased	0.27	0.34

KEGG code#	Dysregulated metabolites in PVS	Direction of dysregulation	Fold change	
			CD	GF
C00581	Guanidinoacetic acid	Increased	1.79	2.15
C00037	Glycine	Increased	1.61	2.12
C00245	Taurine	Increased	1.56	1.47
C03137	N-acetyltryptophan	Increased	1.50	1.99
C00327	Citrulline	Increased	1.35	1.50
C00158	Citric acid	Increased	1.28	1.33
C00047	L-Lysine	Increased	1.28	1.54
C03761	3-Hydroxymethylglutaric acid	Increased	1.21	1.53
C00031	D-Glucose	Decreased	0.62	0.77
C00214	Thymidine	Decreased	0.62	0.37
C00526	Deoxyuridine	Decreased	0.56	0.28
C00491	L-Cystine	Decreased	0.36	0.24
C05598	Phenylacetylglycine	Decreased	0.14	0.11
C05629	Hydrocinnamic acid	Decreased	0.07	0.05
HMDB02302	3-Indolepropionic acid	Decreased	0.04	0.06
HMDB00682	Indoxyl sulfate	Decreased	0.00	0.00

Table S3, related to Figure 4 and S4: Microbiome-dependent metabolites.

Dysregulated metabolites in liver: LC-MS metabolomics identified hepatic metabolites significantly altered 30 min following either saline or pyruvate administration between control mice and microbiome-deficient mice (CD and GF). * denotes putative metabolite identities (*n* = 3-6).

Dysregulated metabolites in PVS: LC-MS metabolomics identified PVS metabolites significantly altered between control mice and microbiome-deficient mice (CD and GF). # Where KEGG codes were not identified, HMDB codes are provided (*n* = 4-5). Fold change was determined as the ratio of CD or GF mean metabolite levels compared to control.

MetaboAnalyst: Microbiome-dependent pathways in liver					
KEGG code	**Dysregulated pathway**	**Number of dysregulated metabolites**		***P*-value**	
		Saline	Pyruvate	Saline	Pyruvate
ko00250	Alanine, aspartate and glutamate metabolism	2	3	***0.004***	***0.001***
ko00471	D-Glutamine/D-Glutamate metabolism	1	1	***0.021***	***0.038***
ko00330	Arginine and proline metabolism	3	1	***0.001***	0.294
ko00970	Aminoacyl-tRNA biosynthesis	3	1	***0.002***	0.424
ko00020	Citrate cycle (TCA cycle)		3		***0.000***
ko00620	Pyruvate metabolism		3		***0.013***
ko00260	Glycine, serine and threonine metabolism	1	2	0.125	***0.023***
ko00230	Purine metabolism	2	1	***0.038***	0.419
ko00680	Methane metabolism	1	1	***0.038***	0.068

XCMS: Microbiome-dependent dysregulated pathways in liver	**Altered, %**	***P*-value**
Myo-inositol *de novo* biosynthesis	100	***0.006***
Glycine biosynthesis	100	***0.006***
4-hydroxyproline degradation	50	***0.007***
β-alanine degradation	67	***0.012***
L-cysteine degradation II	67	***0.012***
L-cysteine degradation I	67	***0.012***
Methylglyoxal degradation I	67	***0.012***
Alanine biosynthesis/degradation	67	***0.012***
Morphine biosynthesis	67	***0.012***
Glycolysis	40	***0.029***

XCMS: Microbiome-dependent dysregulated pathways in PVS	**CD Altered, %**	**GF Altered, %**	**CD *P*-value**	**GF *P*-value**
Ketolysis	100	83	***0.000***	***0.001***
TCA cycle	44	78	***0.001***	***0.001***
Valine degradation	43	80	***0.002***	***0.001***
4-aminobutyrate degradation	50	80	***0.007***	***0.001***
Glycine biosynthesis	50	75	***0.007***	***0.003***
Ascorbate recycling (cytosolic)	50	60	***0.007***	***0.004***
Pyrimidine ribonucleosides degradation	50	43	***0.007***	***0.013***
4-hydroxy-2-nonenal detoxification	50	67	***0.007***	***0.018***
Methylglyoxal degradation I	40	50	***0.012***	***0.035***
Methylglyoxal degradation VI	40	50	***0.012***	***0.035***
Arsenate detoxification I (glutaredoxin)	40	50	***0.012***	***0.035***
Pyrimidine deoxyribonucleosides degradation	40	50	***0.012***	***0.035***
D-glucuronate degradation	40	50	***0.012***	***0.035***

Table S4, related to Figure 4 and S4: Microbiome-dependent pathways.

MetaboAnalyst: Microbiome-dependent pathways in liver: Pathways identified by MetaboAnalyst as being significantly dysregulated ($P < 0.05$), with an impact score > 0, utilizing metabolites listed in Table S3 (saline and pyruvate entered separately). Number of dysregulated metabolites denotes the number of metabolites in the pathway map that are differentially regulated; Blank cells indicate the absence of dysregulated metabolites in the pathway ($n = 3$-6).

XCMS: Microbiome-dependent dysregulated pathways in liver: Unbiased determination of microbiome-dependent hepatic pathways altered by pyruvate stimulation. XCMS analysis of LC-MS metabolomics using pairwise comparisons in the negative ionization mode (no pathways were significantly altered in the positive ionization mode). Microbiome-dependent pathways were defined as metabolic pathways significantly ($P < 0.05$ pyruvate *vs.* saline) altered in conventional control mice but not in microbiome-deficient mice (CD and GF). Percentage of altered metabolites from the total metabolites measured per pathway ($n = 3$-6).

XCMS: Microbiome-dependent dysregulated pathways in PVS: Unbiased determination of microbiome-dependent metabolic pathways altered in the PVS. XCMS analysis of LC-MS metabolomics using pairwise comparisons in the negative ionization mode. Microbiome-dependent pathways were defined as metabolic pathways significantly ($P < 0.05$) altered between control mice and microbiome-deficient mice (CD and GF). Percentage of altered metabolites from the total metabolites measured per pathway ($n = 4$-5).